
# Modeling the Atmospheric Response to Irrigation in the Great Plains. Part I: General Impacts on Precipitation and the Energy Budget

KEITH J. HARDING AND PETER K. SNYDER

*Department of Soil, Water, and Climate, University of Minnesota, St. Paul, Minnesota*

(Manuscript received 12 August 2011, in final form 13 June 2012)

ABSTRACT

Since World War II, the expansion of irrigation throughout the Great Plains has resulted in a significant decline in the water table of the Ogallala Aquifer, threatening its long-term sustainability. The addition of near-surface water for irrigation has previously been shown to impact the surface energy and water budgets by modifying the partitioning of latent and sensible heating. A strong increase in latent heating drives near-surface cooling and an increase in humidity, which has opposing impacts on convective precipitation. In this study, the Weather Research and Forecasting Model (WRF) was modified to simulate the effects of irrigation on precipitation. Using a satellite-derived fractional irrigation dataset, grid cells were divided into irrigated and nonirrigated segments and the near-surface soil layer within irrigated segments was held at saturation. Nine April–October periods (three drought, three normal, and three pluvial) were simulated over the Great Plains. Averaging over all simulations, May–September precipitation increased by 4.97 mm (0.91%), with localized increases of up to 20%. The largest precipitation increases occurred during pluvial years (6.14 mm; 0.98%) and the smallest increases occurred during drought years (2.85 mm; 0.63%). Precipitation increased by 7.86 mm (1.61%) over irrigated areas from the enhancement of elevated nocturnal convection. Significant precipitation increases occurred over irrigated areas during normal and pluvial years, with decreases during drought years. This suggests that a soil moisture threshold likely exists whereby irrigation suppresses convection over irrigated areas when soil moisture is extremely low and enhances convection when antecedent soil moisture is relatively high.

## 1. Introduction

The expansion of irrigation in the Great Plains since World War II has significantly affected the Ogallala Aquifer—a shallow aquifer that stretches from the Texas Panhandle to South Dakota (Fig. 1). Large withdrawals from the Ogallala Aquifer have resulted in declines in the water table by more than 40 m (McGuire 2007), making extraction for municipal and agricultural uses more expensive (McGuire et al. 2003) and jeopardizing the viability of future groundwater extraction. Irrigation is heavily concentrated within and adjacent to the Ogallala Aquifer as identified by United States Department of Agriculture (USDA) and satellite-derived irrigation estimates (Ozdogan and Gutman 2008). In some areas, up to 80% of the land has been irrigated since predevelopment (Mahmood et al. 2006), roughly doubling water available for evapotranspiration (ET) within the domain of the Ogallala Aquifer (Moore and Rojstaczer 2001). Most of the water applied to the surface through irrigation is evapotranspired rather than being lost through runoff or drainage (DeAngelis et al. 2010; Moore and Rojstaczer 2001). This results in changes to the atmospheric branch of the hydrologic cycle as the evapotranspired water eventually falls out as precipitation.

The goal of this study is to explore the impact that irrigation has on the hydrologic cycle using a high-resolution coupled land–atmosphere model. Simulations using the Weather Research and Forecasting Model (WRF; Skamarock et al. 2008) were performed both with and without irrigation for a suite of years for different precipitation regimes. This includes El Niño–Southern Oscillation (ENSO) years that have a marked influence on Great Plains precipitation (Twine et al. 2005).

The availability of such a large quantity of water for ET has a sizeable effect on surface energy and water budgets (Pielke 2001). Increases in latent heating with additional water are offset by decreases in sensible heating, resulting in changes to the surface temperature

*Corresponding author address:* Peter K. Snyder, Department of Soil, Water, and Climate, 439 Borlaug Hall, 1991 Upper Buford Circle, Saint Paul, MN 55108.
E-mail: pksnyder@umn.edu

DOI: 10.1175/JHM-D-11-098.1

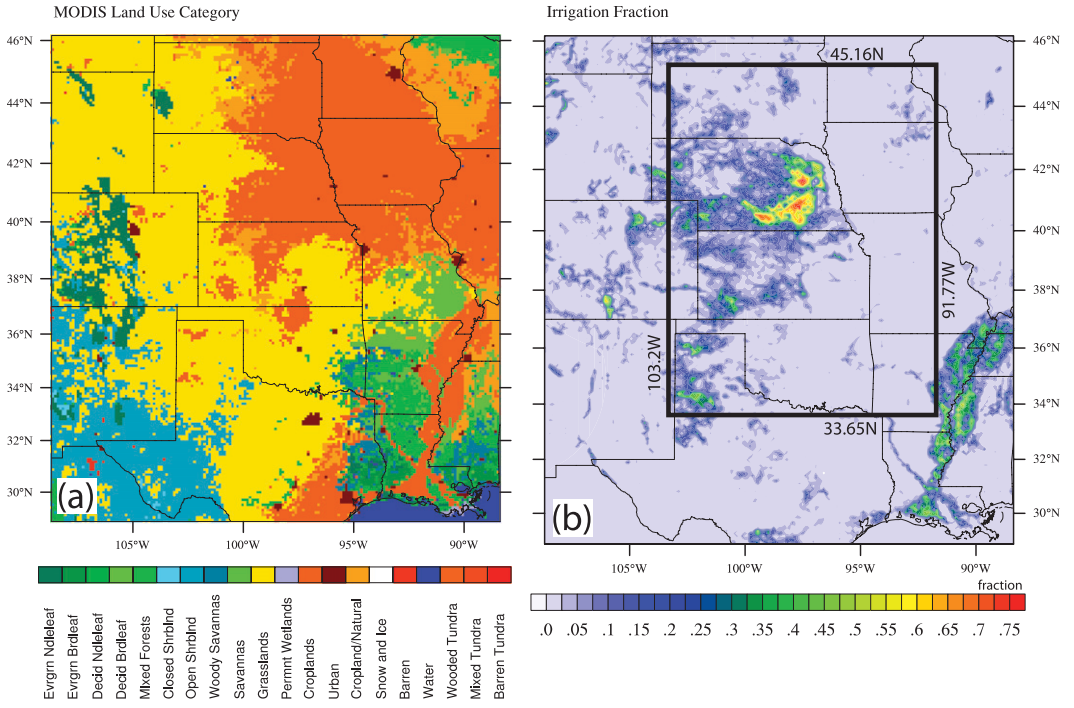


FIG. 1. (a) The dominant MODIS land use category used as input to WRF and (b) the irrigated fraction from Ozdogan and Gutman (2008) over the WRF domain. The region of study shown in (b) is a subset of the WRF domain chosen to minimize model edge effects.

and moisture fields (Barnston and Schickedanz 1984; DeAngelis et al. 2010; Kueppers et al. 2007; Ozdogan et al. 2010; Pielke 2001; Sacks et al. 2009). The repartitioning of net radiation into latent heating at the expense of sensible heating decreases the surface air temperature and increases the surface dewpoint temperature as shown by numerous modeling and observational studies (Adegoke et al. 2003; Baidya Roy et al. 2003; Kueppers et al. 2007; Lobell et al. 2006; Mahmood et al. 2004, 2006; Sacks et al. 2009). Mahmood et al. (2006) observed a mean surface temperature decrease of approximately 1°C over the growing season for heavily irrigated sites in Nebraska during the second half of the twentieth century while Baidya Roy et al. (2003) simulated a cooling of up to 1°C over the Great Plains and Midwest using a regional model. Similarly, Mahmood et al. (2006) observed a seasonally averaged 4°–5°C dewpoint temperature difference between irrigated and nonirrigated sites in Nebraska while Adegoke et al. (2003) simulated a dewpoint increase of 2.6°C over Nebraska in July.

Convective precipitation develops when sufficient quantities of convective available potential energy (CAPE), precipitable water, and a lifting mechanism occur in the presence of a sufficiently thick planetary boundary layer (PBL) and relatively small amounts of convective inhibition (CIN; Bluestein 1993). Changes in the surface temperature and moisture fields with irrigation have opposing effects on the development of convective precipitation. Additional near-surface moisture from irrigation enhances convection by increasing CAPE, despite lower temperatures with irrigation (Crook 1996; Pielke 2001; Segal et al. 1998) because CAPE is more dependent on changes in low-level moisture than temperature (Crook 1996). However, surface cooling and enhanced cloud cover from irrigation also increase CIN, which is more sensitive to changes in temperature than moisture (Crook 1996), inhibiting the development of deep convection (Barnston and Schickedanz 1984; Boucher et al. 2004; De Ridder and Gallée 1998; DeAngelis et al. 2010; Sacks et al. 2009). Findell and Eltahir (2003b) showed that reduced sensible heating over moist soils can suppress the vertical growth of the PBL enough to prevent turbulent eddies from reaching the level of free convection (LFC). This was shown to frequently occur over the southern Great Plains in the presence of a dry lower troposphere and steep lapse rates (Findell and Eltahir 2003a). Over irrigated areas where localized cooling occurs, the suppression of convection from decreased PBL heights and increased CIN is especially magnified (DeAngelis et al. 2010; Sacks et al. 2009). DeAngelis et al. (2010) proposed that locations downwind of irrigated areas experience

increases in CAPE without increases in CIN because while additional moisture is advected in from irrigated regions, temperature decreases do not occur in the absence of latent cooling. When synoptic conditions are favorable for the forcing of convection, an increase in CAPE downwind of irrigated locations enhance convective precipitation. Because a large percentage of precipitation over the Great Plains is driven by convection [80% of July and August precipitation over the Ogallala Aquifer domain (Changnon 2001)], it is reasonable to assume that increased CAPE with irrigation will contribute to greater precipitation.

The addition of low-level moisture from irrigation increases precipitation not only through enhanced convection, but also through an increase in precipitable water (Boucher et al. 2004). Koster et al. (2004) noted that soil moisture is positively correlated with precipitation over the Great Plains. Increased soil moisture drives an increase in ET, thereby providing the atmosphere with additional precipitable water, which has been shown to be positively correlated with precipitation at both global and regional scales (Trenberth et al. 2003). Because CAPE and precipitable water increase with irrigation, precipitation increases are expected to occur downwind of irrigated areas provided that the forcing for convection (i.e., low-level convergence, moisture flux convergence, and upper-level divergence) is unchanged (Banacos and Schultz 2005; DeAngelis et al. 2010).

Numerous observational studies have attempted to determine the impact of irrigation on precipitation, with generally contradictory results. Barnston and Schickedanz (1984) observed a precipitation increase of up to 20% over the Texas Panhandle from 1930 to 1970, coincident with the rapid adoption of irrigation. Contrarily, Moore and Rojstaczer (2001) were unable to attribute changes in precipitation to irrigation over the Great Plains from 1950 to 1982 using an EOF analysis of precipitation. DeAngelis et al. (2010) observed an increase in July precipitation downwind of irrigated areas over the Ogallala Aquifer with the rapid adoption of irrigation. Similarly, Jódar et al. (2010) observed orographic precipitation increases downwind of irrigated areas in Spain.

Observational studies have yielded contradictory results partly because they have been conducted for periods when irrigation expansion was too small to influence precipitation or they took place over small areas where downwind effects cannot be realized (DeAngelis et al. 2010). Additionally, the exact impact of irrigation cannot be isolated from numerous compounding climatic factors. Simulating the precipitation response from irrigation can be used to overcome observational limitations by controlling for climate variability. Previous studies have found a generally consistent precipitation response to irrigation using mesoscale models (Pielke et al. 1997; Segal et al. 1998), regional atmospheric models (Adegoke et al. 2003; Baidya Roy et al. 2003; De Ridder and Gallée 1998), global climate models (GCMs; Lee et al. 2011; Puma and Cook 2010; Sacks et al. 2009), and offline land surface models (LSMs; Ozdogan et al. 2010). Segal et al. (1998) simulated a slight increase in precipitation over North America while Sacks et al. (2009) simulated a 1.24% June–August increase in precipitation globally over land. De Ridder and Gallée (1998) simulated conditions that favored increased moist convective development in southern Israel.

Limited computational resources have prevented many models from being run at sufficiently high spatial resolutions to adequately resolve small-scale land–atmosphere interactions and mesoscale convection (Segal et al. 1998). Modeling studies run at coarse spatial resolutions over large areas provide a good sense of the general impacts of irrigation on precipitation, but higher resolutions are needed to fully resolve the processes that influence precipitation in regions dominated by convection. Similarly, studies that were run at high spatial resolution were implemented over small domains for short time periods, yielding results that do not include downwind effects or are not applicable outside of the simulated periods.

Models have been used to simulate irrigation with varying levels of complexity. Using a regional climate model, Kueppers et al. (2007) held the soil at field capacity for all irrigated grid cells in California, while Adegoke et al. (2003) saturated all irrigated grid cells once daily in Nebraska. Sacks et al. (2009) applied water to the cropland fraction of grid cells when the leaf area index (LAI) reached 80% of the annual maximum. Puma and Cook (2010) applied soil moisture to the vegetated portion of irrigated grid cells whenever soil moisture dropped below crop-dependent thresholds, while Ozdogan et al. (2010) used a daily irrigation trigger to determine whether to irrigate.

In this study, WRF was run over the Great Plains at a 10-km spatial resolution while holding the irrigated portion of grid cells at saturation—an approach similar to Adegoke et al. (2003) but with the addition of subgrid-scale irrigation similar to Puma and Cook (2010) and Sacks et al. (2009). This experimental design allows for determination of the upper limits of the impact that irrigation has on precipitation and the energy and water budgets over the Great Plains. Various climatic regimes were chosen to represent a variety of precipitation conditions that influence the warm-season climate of the Great Plains. This approach can be used to assess the

general impact of irrigation on the climate of the Great Plains and whether these impacts vary with different precipitation regimes.

## 2. Methods

### a. WRF–Noah model description

The regional WRF version 3.2 (Skamarock et al. 2008) was used to simulate the atmospheric response to irrigation. WRF is a mesoscale and nonhydrostatic atmospheric model that can be used both for research and operational forecasting. The model uses a terrain-following vertical coordinate system that extends from the surface to 50 hPa. The Noah LSM, which has been coupled to WRF, was used to provide surface fluxes of energy, momentum, and mass to WRF.

The Noah LSM includes a static vegetation component with four soil layers and one canopy layer. The LSMs currently coupled to WRF do not include dynamic vegetation. While vegetation in Noah influences the atmosphere, it does not change in response to the atmospheric conditions provided by WRF, and thus only one-way feedbacks can be examined. Vegetation and soil parameters and land cover data were assimilated into Noah from the 20-category, 30-arc-second-resolution Moderate Resolution Imaging Spectroradiometer (MODIS) land use dataset (Friedl et al. 2002). Because Noah represents vegetation statically, LAI is forced to follow the same annual cycle observed by MODIS and does not respond to atmospheric conditions. ET is calculated as the sum of direct ground and canopy evaporation, transpiration from vegetation, and sublimation (Chen and Dudhia 2001; Hong et al. 2009), all of which are calculated through simple linear methods using soil and vegetation parameters based on MODIS (Betts et al. 1997; Friedl et al. 2002; Jacquemin and Noilhan 1990; Noilhan and Planton 1989).

### b. Irrigation representation

Irrigation was represented on a subgrid cell basis to capture the small-scale heterogeneity of irrigation without being computationally prohibitive or resulting in the breakdown of the model physics. The fraction of irrigation in each grid cell was obtained from the 500-m-resolution MODIS-derived fractional irrigation dataset from Ozdogan and Gutman (2008) and aggregated to a 10-km domain (Fig. 1). The MODIS irrigation dataset represents the fractional irrigation area from 2001 and is highly correlated to the 2002 USDA–National Agricultural Statistics Service (NASS) irrigation dataset on a state level ($R^2 = 0.8833$) (NASS 2002). The MODIS-derived dataset was chosen because it is based on observations whereas the USDA–NASS dataset was compiled from county-level reports that may be subject to more errors or missing data.

The Noah LSM was modified to calculate surface fluxes based on the soil moisture in the irrigated and nonirrigated parts of each grid cell. Irrigation was simulated by applying water directly to the soil surface of the irrigated portion of each grid cell and maintaining the soil moisture at saturation to a depth of 2 m. The soil moisture in the nonirrigated portion was controlled by the unmodified physics of the Noah LSM. Because the static vegetation cannot respond to the increase in soil moisture with irrigation, an increase in ET can only occur in response to reduced plant moisture stress and soil evaporation, not from accentuated plant growth.

MODIS land use categories were left unchanged and irrigation was applied based on the fractional irrigation dataset from Ozdogan and Gutman (2008). Surface fluxes and variables for each grid cell were calculated separately for the irrigated and nonirrigated portions of a grid cell at each time step and were weighted based on the irrigated fraction as shown in Eq. (1):

$$H = f_i H_{\text{irrigated}} + (1 - f_i) H_{\text{non irrigated}}, \qquad (1)$$

where $H$ is the sensible heat flux for a grid cell, $f_i$ is the irrigated fraction, $H_{\text{irrigated}}$ is the sensible heat flux over the irrigated portion of a grid cell, and $H_{\text{non irrigated}}$ is the sensible heat flux over the nonirrigated portion. The areal extent and amount of irrigation were kept constant from April to September, overlapping the period of heaviest annual irrigation in the Great Plains (DeAngelis et al. 2010). Because the soil moisture was kept at saturation, this resulted in the overuse of irrigated water compared to reality. For example, for Colorado, Kansas, and Nebraska, water use for irrigation for May–September 2000 in WRF was $7.06 \times 10^{10}$ m$^3$, which is slightly more than double USDA annual irrigation surface and groundwater withdrawals of $3.3 \times 10^{10}$ m$^3$ (Hutson et al. 2004). Such a simplistic and somewhat aggressive irrigation scheme was necessary because with realistic (lower) application amounts the additional transpiration over irrigated areas from accentuated plant growth will not occur with static vegetation and the total ET will be lower than observed. Such shortcomings could be reduced with the inclusion of a dynamic vegetation model in WRF, but because no such model is currently available, the irrigation approach used here is deemed adequate.

### c. Experimental design

This study includes three precipitation regimes representing the range of climatic and antecedent soil

TABLE 1. Summary of precipitation regimes used in this study. ENSO events are listed for years with notable precipitation anomalies.

| Simulations | Precipitation regimes | | |
|---|---|---|---|
| | Drought | Normal | Pluvial |
| Current vegetation, irrigated (IRRIG) | 1983 (El Niño) | 1997 | 1993 (El Niño) |
| | 2000 | 1990 | 2008 (Neutral) |
| | 1988 (La Niña) | 1985 | 2007 |
| Current vegetation, nonirrigated (CONTROL) | 1983 (El Niño) | 1997 | 1993 (El Niño) |
| | 2000 | 1990 | 2008 (Neutral) |
| | 1988 (La Niña) | 1985 | 2007 |

moisture conditions observed over the Great Plains. The characterization of drought, normal, and pluvial years was determined by calculating the 1980–2008 average May–September precipitation for the region of study (Fig. 1b) using the North American Regional Reanalysis (NARR) dataset (Mesinger et al. 2006). Drought years were identified as being at least one standard deviation below the 1980–2008 mean while pluvial years were identified as being at least one standard deviation above the mean. Normal years were identified as being within one standard deviation of the mean. Nine hydrologically unique years were then chosen to represent the three precipitation regimes (Table 1).

Determination of the model parameters was based on the performance of 14 simulations of WRF without irrigation from 1 to 30 June 2005—a normal precipitation and neutral ENSO year. Simulations incorporated a variety of spatial and temporal resolutions, domain sizes, and model parameters to achieve a suitable array of possible model configurations. The model configuration used in this study was based on the performance of the simulated precipitation compared to National Centers for Environmental Prediction (NCEP) Stage IV (Lin and Mitchell 2005) and Climate Prediction Center (CPC)'s Unified Precipitation (Higgins et al. 2000) datasets, the computational efficiency of the model, and the capability of the model to resolve physical processes between the land surface and the atmosphere.

WRF was initialized using 3-hourly data from NARR for all identified years in Table 1. All model simulations were completed using the same $180 \times 195$ grid with a 10-km horizontal resolution, 38 vertical levels, and a 30-s time step (except for 2007, which had a 25-s time step because of instabilities with the forcing dataset during that year). Control (CTRL) and irrigation (IRRIG) simulations were run for each year from 1 April to 1 October, overlapping the period of heaviest annual irrigation in the Great Plains (DeAngelis et al. 2010). The Morrison two-moment microphysics scheme (Morrison et al. 2009), Yonsei University (YSU) planetary boundary layer (PBL) scheme (Hong et al. 2006), Rapid Radiative Transfer Model (RRTM) longwave radiation scheme (Mlawer et al. 1997), Dudhia shortwave radiation scheme (Dudhia 1989), and fifth-generation Pennsylvania State University–National Center for Atmospheric Research Mesoscale Model (MM5) surface-layer scheme were used (Skamarock et al. 2008). No cumulus parameter was employed.

Depending on the model configuration, the exclusion of a cumulus parameter (CP) can result in difficulties initiating and resolving deep convection (Kain et al. 2008), generally leading to less precipitation compared to observations. However, based on a suite of sensitivity simulations for April–September 1997 compared to the CPC dataset, including a CP actually led to a large overestimation of precipitation by 83% as compared to 11% without a CP. Analysis of these results suggests that convective overturning is sufficiently resolved for this model configuration and the exclusion of a CP produces precipitation estimates that are closer to observations. To test whether the NARR forcing dataset was responsible for the overestimation of precipitation and not the exclusion of a CP, additional simulations were run with the NCEP–Department of Education (DOE) reanalysis (Kanamitsu et al. 2002). Over April–September 1997, the simulated precipitation using a CP was overestimated by 58%, compared to only 10% for an identical simulation without a CP (not shown), suggesting that the overestimation of precipitation was independent of the forcing dataset.

Considering the precipitation that fell within the region of study as shown in Fig. 1b for May–September of all simulated years, WRF overestimated precipitation by 19.0% when using the selected model configuration for the average of all simulated years (Fig. 2) compared with the CPC dataset (Higgins et al. 2000). While WRF overestimated precipitation, the model simulated the west–east precipitation gradient that is present over the Great Plains in the CPC dataset reasonably well (Fig. 2). Because this overestimation was similar for both irrigation and control simulations, the results contained no systematic bias.

### *d. Statistical significance*

Student's *t* tests using a matched pairs design were employed to test for statistical significance when

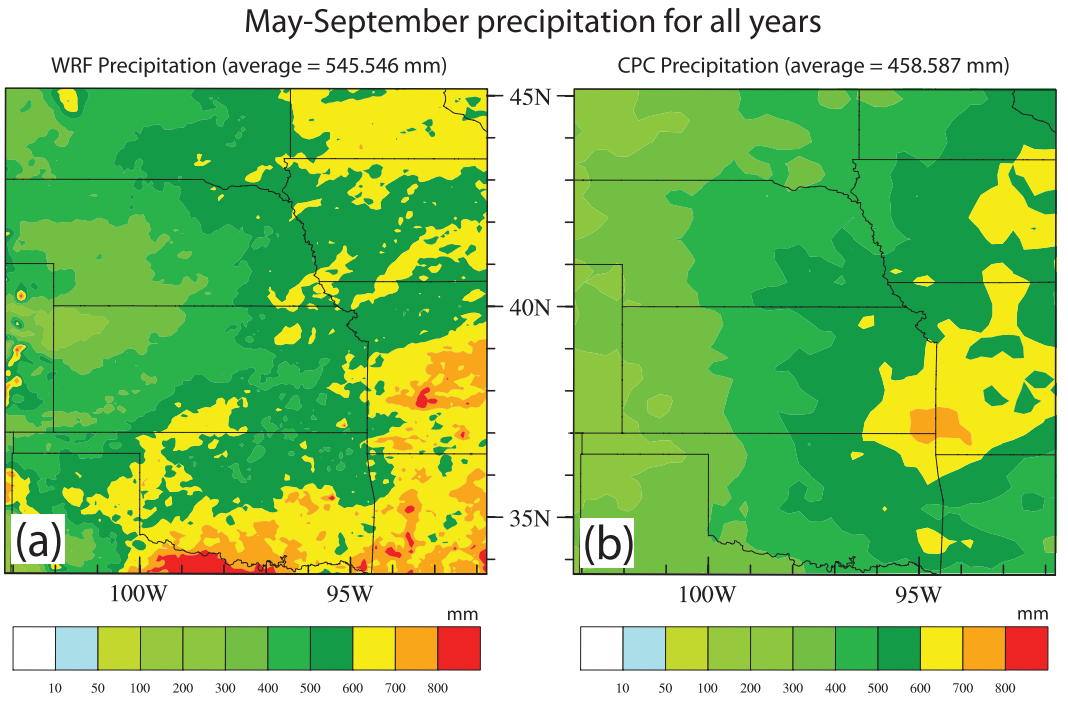


FIG. 2. (a) Average May–September control (no irrigation) simulated precipitation (mm) from WRF for all years. (b) Average May–September precipitation (mm) from the CPC U.S. Unified Precipitation dataset for the same years as in (a) (Higgins et al. 2000).

comparing variables between control and irrigation simulations. In a matched pairs design, the control and treatment (irrigated) groups share the same variance between individual samples and only the variance of the difference between the groups is considered so as to avoid testing on shared variance (interannual variability) between groups. In this study, the set of differences is considered to be the set of control simulations subtracted from the set of irrigation simulations, unless otherwise noted. All *t* tests were performed using two tails with a 95% confidence level, unless otherwise noted.

## 3. Results

All results are reported for the region of study (as shown in Fig. 1b) using area-weighted averages over the domain for all simulated years from May to September unless otherwise noted.

### *a. Model validation*

Assessment of WRF's ability to simulate the impact of irrigation on surface fluxes is determined from comparison of monthly averages of observations from two Ameriflux sites near Mead, Nebraska, for 2002–09 with WRF averages for all simulated years from a grid cell in WRF centered 8 km from the Ameriflux sites. Comparison of the monthly average latent heat flux values from each Amerflux site with WRF shows a general overestimation of latent heating by WRF. Control simulations of WRF show an overestimation of the latent heat flux by 19.1% compared with the Ameriflux Mead rainfed site (41.1797°N, 96.4396°W; Fig. 3a) (Verma et al. 2005), while irrigation simulations of WRF overestimate latent heating by 15.8% compared with the Ameriflux Mead irrigated rotation site (41.1649°N, 96.4701°W; Fig. 3b) (Verma et al. 2005). Given that eddy-covariance methods generally underestimate latent heating on the order of 20% when closure of the energy budget is not achieved (as was the case with these two sites) (Twine et al. 2000; Wilson et al. 2002), it is reasonable to assume that the observed latent heating is likely higher than measured and more in agreement with WRF. When considering the individual sites (Figs. 3a,b), WRF simulates the seasonality of latent heating, but not the seasonality of the difference between the sites. However, the seasonally averaged difference simulated by WRF is 6.20 W $m^{-2}$ compared with an observed difference of 7.74 W $m^{-2}$, suggesting that WRF adequately represents the effect of irrigation on latent heating on seasonal time scales. Despite the fact that WRF underestimates the seasonal average of the difference in sensible heating (Fig. 3f), WRF performs reasonably well in capturing the seasonality and seasonal average of the 2-m temperature difference (Fig. 3l). Similarly, WRF simulates the seasonality of net radiation

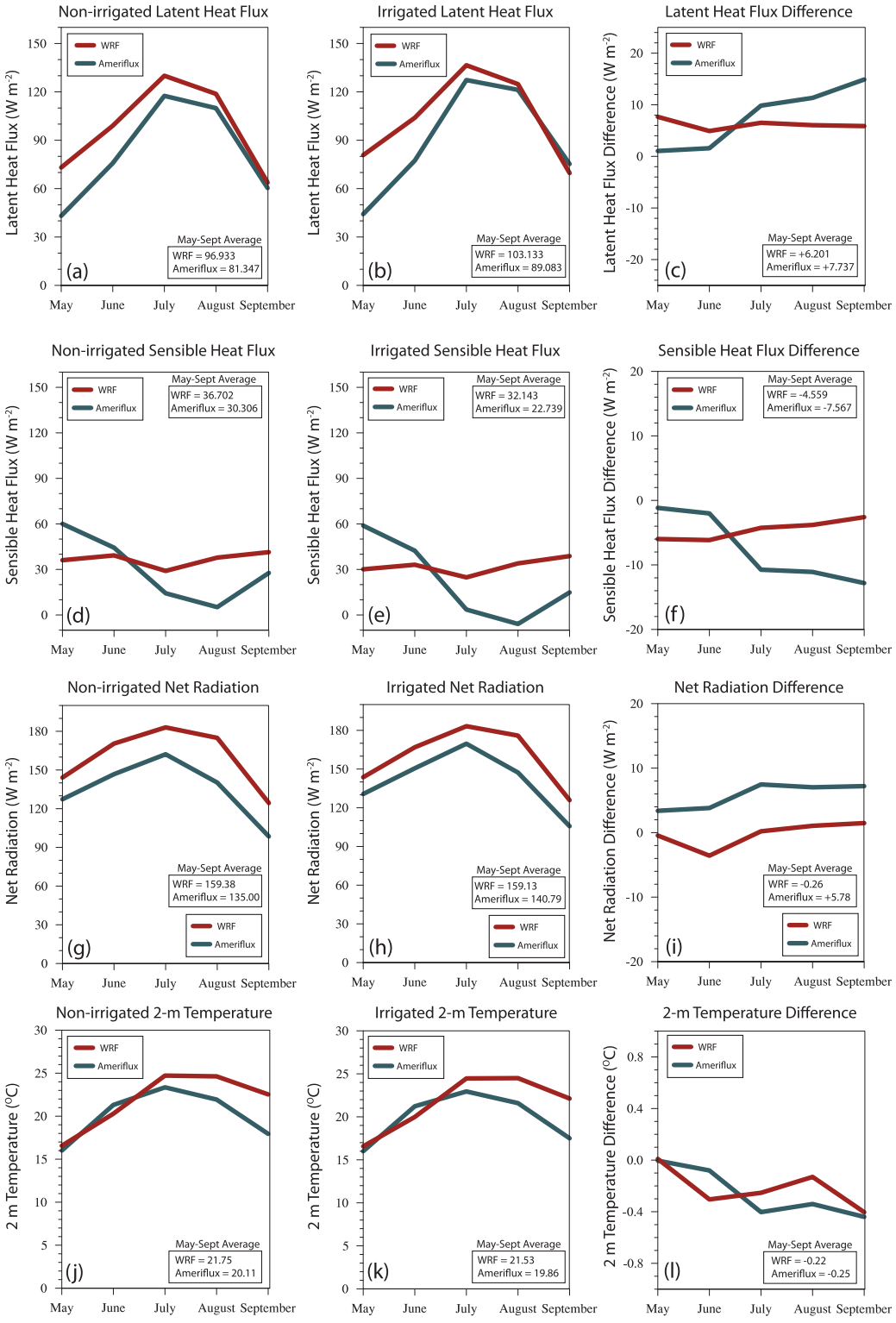


FIG. 3. (a) Monthly averaged latent heat flux (W $m^{-2}$) observed at Ameriflux Mead rainfed site for 2002–09 (blue) and simulated by WRF at a grid cell (centered 8 km from the Ameriflux site locations) in control simulations for all simulated years (red). (b) As in (a), but observed at Ameriflux Mead irrigated rotation site (blue) and simulated by WRF with irrigation (red). (c) As in (a), but for latent heat flux difference (W $m^{-2}$) between Ameriflux Mead irrigated rotation and rainfed sites (blue) and WRF irrigated and control simulations (red). (d)–(f) As in (a)–(c), but for sensible heat flux (W $m^{-2}$) . (g)–(i) As in (a)–(c), but for net radiation (W $m^{-2}$) . (j)–(l) As in (a)–(c), but for 2-m temperature (°C).

TABLE 2. May–September area-weighted averages of differences between control and irrigated simulations for all simulated years. Area-weighted averages were calculated for the region of study, for grid cells with at least 10% irrigation within the region of study, and for grid cells with less than 10% irrigation within the region of study. Significance values for paired $t$ tests are as follows: * ($p < 0.1$), ** ($p < 0.05$), and *** ($p < 0.01$).

| | Region of study (RoS) averages | 10%+ irrigated grid cells within RoS | Grid cells with < 10% irrigation within RoS |
|---|---|---|---|
| Irrigated area ($km^2$) | $6.39 \times 10^4$ | $5.0 \times 10^4$ | $1.83 \times 10^4$ |
| Soil moisture difference ($m^3\ m^{-3}$) | 0.014 (5.68%)*** | 0.059 (27.0%)*** | $5.61 \times 10^{-3}$ (2.27%)*** |
| Latent heat flux change ($W\ m^{-2}$) | 4.293 (4.29%)*** | 20.745 (22.6%)*** | 1.305 (1.28%)*** |
| Sensible heat flux change ($W\ m^{-2}$) | −3.235 (−7.74%)*** | −14.542 (−30.2%)*** | −1.182 (−2.91%)*** |
| Net radiation change ($W\ m^{-2}$) | 0.107 (0.06%) | 1.580 (0.94%)** | −0.160 (−0.09%) |
| 2-m temperature change (°C) | −0.159* | −0.485*** | −0.100 |
| 2-m mixing ratio ($g\ kg^{-1}$) | 0.191 (1.79%)*** | 0.519 (5.24%)*** | 0.131 (1.22%)*** |
| Precipitable water change (mm) | 0.137 (0.50%)*** | 0.186 (0.74%)*** | 0.128 (0.46%)*** |
| CAPE change ($J\ kg^{-1}$) | 16.128 (5.01%)*** | 45.099 (16.0%)*** | 10.866 (3.30%)*** |
| CIN change ($J\ kg^{-1}$) | 0.214 (0.61%) | 2.091 (5.71%)* | −0.127 (−0.37%) |
| PBL height change (m) | −23.533 (−2.88%)*** | −67.854 (−7.80%)*** | −15.483 (−1.92%)*** |
| LFC change (m) | −154.88 (−2.22%)*** | −333.48 (−4.61%)*** | −122.45 (−1.77%)*** |
| Convergence change ($s^{-1}$) | $-3.27 \times 10^{-9}$ (−4.75%)* | $-8.87 \times 10^{-8}$ (−84.2%)*** | $1.224 \times 10^{-9}$ (19.6%)*** |
| Precipitation change (mm) | 4.974 (0.91%)** | 7.861 (1.61%) | 4.449 (0.80%)** |

(Figs. 3g,h) and 2-m temperature (Figs. 3j,k), with considerably less accuracy when considering sensible heating (Figs. 3d,e). Because WRF captures the seasonality in the surface energy budget terms and temperature with irrigation, it is determined that the irrigation submodel accurately represents the atmospheric impact of irrigation despite the aggressive and conceptually unrealistic application of moisture to the soil.

### b. *Overall model results*

In the following sections, ''overall'' results refer to May–September area-weighted averages over the entire region of study, while results for ''irrigated grid cells'' refer to May–September area-weighted averages of grid cells with at least 10% irrigation within the region of study, and ''nonirrigated grid cells'' refer to grid cells with less than 10% irrigation.

Soil moisture increases of 27% in irrigated grid cells (Table 2) contribute to statistically significant increases in latent heating (Fig. 4a) and decreases in sensible heating (Fig. 4b). Latent heat flux increases of 20.7 $W\ m^{-2}$ (22.6%) and sensible heat flux decreases of 14.5 $W\ m^{-2}$ (−30.2%) occur in irrigated grid cells (Table 2). The increase in latent heating drives statistically significant increases in 2-m mixing ratio over much of the Great Plains (Fig. 4c; Table 2). Similarly, decreases in sensible heating are coincident with statistically significant decreases in the 2-m temperature in the vicinity of irrigated grid cells (Fig. 4d), with 0.5°C temperature decreases over irrigated grid cells, 0.1°C decreases over nonirrigated grid cells, and 0.2°C decreases overall (Table 2).

The increase in low-level moisture results in statistically significant increases in surface-based CAPE throughout much of the Great Plains (Fig. 5a) with an amplified response over irrigated grid cells (Table 2). The addition of low-level moisture from irrigation leads to statistically significant increases in column precipitable water (Fig. 5d; Table 2) and increases in low-level cloud cover adjacent to irrigated areas (not shown), but net radiation increases slightly (Table 2) because of decreases in upwelling longwave radiation (not shown). Low-level cooling contributes to CIN increases and decreases in the PBL height over much of the Great Plains from low-level cooling (Fig. 5c; Table 2). However, larger declines in the LFC (Table 2) imply that turbulent eddies within the PBL can more easily reach the LFC to initiate convection, suggesting that declines in the PBL height likely do not contribute significantly to suppressing convective precipitation. While increases in CIN are present over irrigated areas throughout the Great Plains, only a small number of irrigated grid cells see increases that are statistically significant (Fig. 5b). Low-level cooling also results in a decrease in surface convergence over irrigated grid cells, with smaller decreases overall, and increases in convergence over nonirrigated grid cells (Table 2).

Statistically significant average precipitation increases of 4.97 mm (0.91%) and 4.25 mm (1.29%) are observed overall for May–September and June–August, respectively (Fig. 6a), with localized precipitation increases of up to 20% over parts of Nebraska, Kansas, and Oklahoma (Fig. 6c). The average overall May–September precipitation increase is smaller than the increase in evapotranspiration (22.70 mm), meaning that irrigation results in a net loss of water by 17.73 mm. On average, precipitation increases are larger for irrigated grid cells compared with the entire region of study and nonirrigated grid cells during

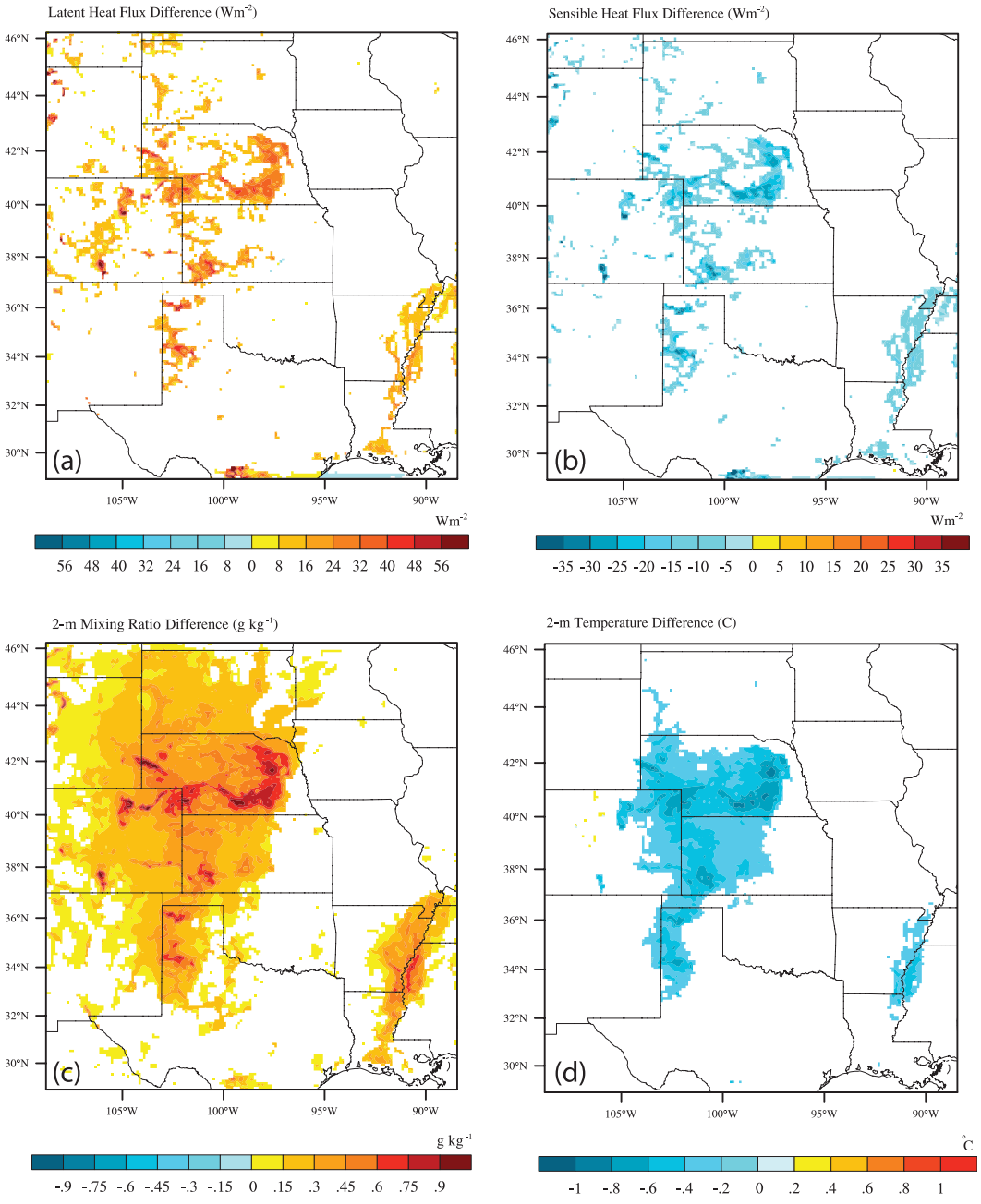


FIG. 4. (a) Average May–September simulated latent heat flux difference (IRRIG minus CTRL) for all years. (b) As in (a), but for sensible heat flux (W $m^{-2}$). (c) As in (a), but for 2-m mixing ratio (g $kg^{-1}$). (d) As in (a), but for 2-m temperature (°C). Differences are shown only for grid cells found to be significant using a two-tailed, paired *t* test at the 95% confidence level.

May–September (Table 2) and June–August (not shown). Precipitation increases over irrigated grid cells primarily occur during the overnight and morning hours (Fig. 7b), when convection tends to be elevated above the nocturnal boundary layer (Wilson and Roberts 2006). Slight decreases occur in the afternoon (Fig. 7b) when convection tends to be more surface based (Wilson and Roberts 2006). This is coincident with the fact that irrigated grid cells exhibit strong decreases in surface convergence and increases in CIN, which inhibits convection during the day but otherwise does not play a role at night. The greatest increases in precipitation over nonirrigated grid cells occur in the afternoon hours (Fig. 7a) when convection tends to be more surface based (Wilson and Roberts 2006), which is

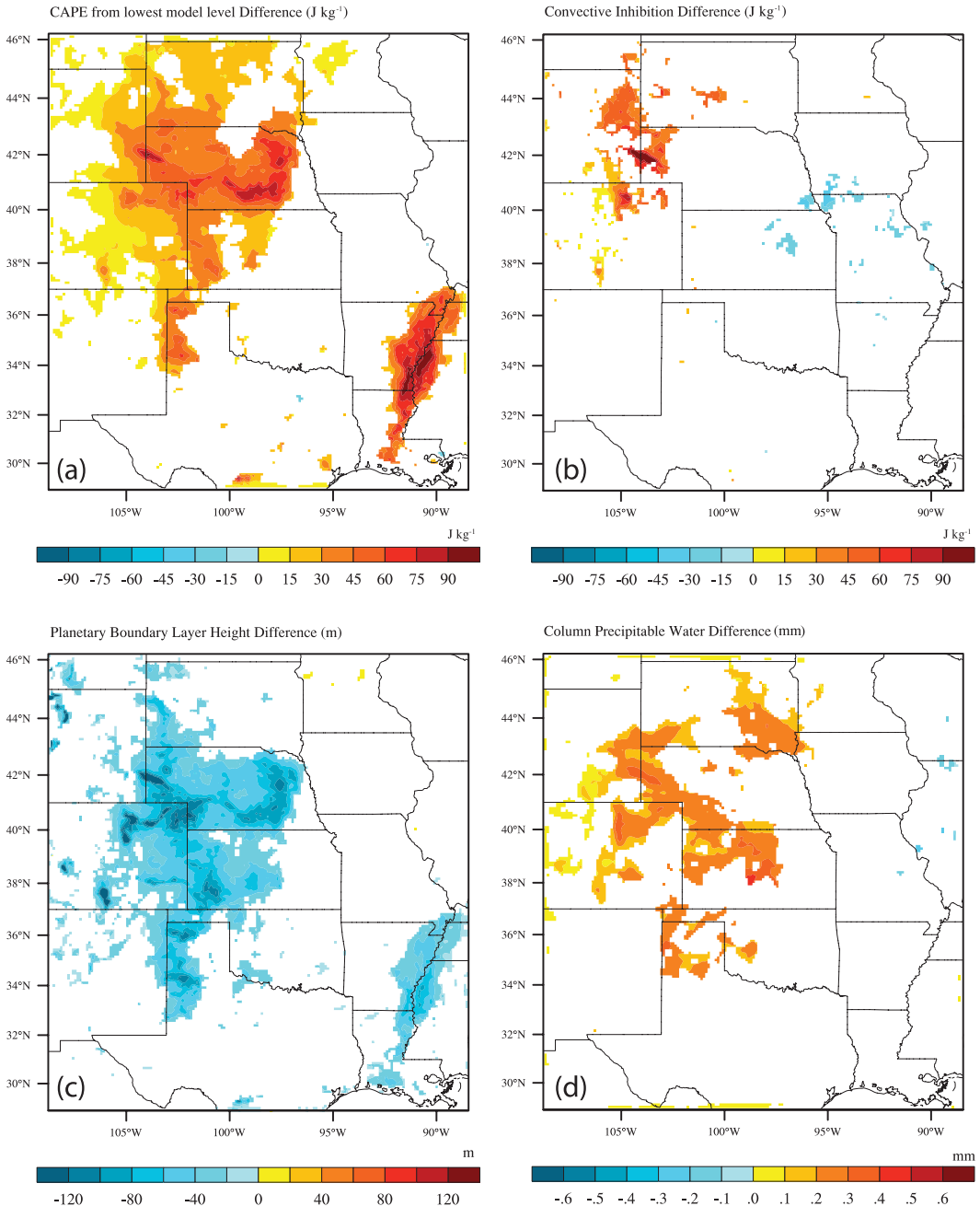


FIG. 5. (a) Average May–September simulated CAPE (J kg$^{-1}$) difference (IRRIG minus CTRL) for all years. (b) As in (a), but for CIN (J kg$^{-1}$). (c) As in (a), but for PBL height (m). (d) As in (a), but for column precipitable water (mm). Differences are shown only for grid cells found to be significant using a two-tailed, paired *t* test at the 95% confidence level.

coincident with strong increases in surface convergence over nonirrigated grid cells. No individual months have statistically significant changes in precipitation (not shown). No individual grid cells have statistically significant changes in precipitation when considering the spatial pattern of precipitation changes from irrigation (Fig. 6c).

The effects of irrigation are amplified with increasing irrigation fraction (Fig. 8). Stronger soil moisture enhancement with increasing irrigation fraction (Fig. 8a) results in greater partitioning of net radiation into latent heating for heavily irrigated grid cells (Fig. 8b), at the expense of sensible heating (Fig. 8c). As a result, surface

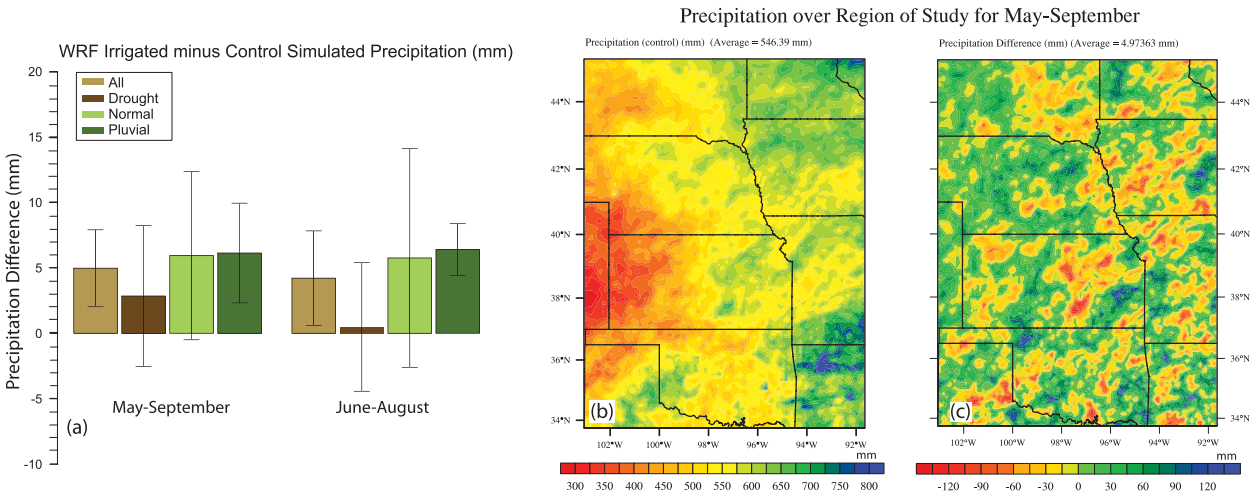


FIG. 6. (a) Area-weighted average of simulated precipitation (mm) difference (IRRIG minus CTRL) over the region of study (defined in Fig. 1b) during June–August (JJA) and May–September for drought, normal, pluvial, and all years. Error bars denote 95% confidence interval. (b) Average May–September CTRL simulated precipitation (mm) for all years. (c) Average May–September IRRIG minus CTRL simulated precipitation (mm) for all years. No differences in (c) were found to be statistically significant using a two-tailed, paired *t* test at the 95% confidence level.

cooling (Fig. 8d) and surface moisture enhancement (Fig. 8e) intensify as irrigation becomes more concentrated. Greater increases in 2-m mixing ratio with increasing irrigation fraction drive larger CAPE increases for heavily irrigated grid cells (Fig. 8f). However, stronger surface cooling with increasing irrigation fraction results in greater CIN increases (Fig. 8g), stronger decreases in convergence (Fig. 8i), and stronger subsidence (not shown) with increasing irrigation intensity. Greater latent heating with increasing irrigation intensity contributes to the enhancement of column precipitable water with increasing irrigation fraction until about 25% irrigation fraction, but decreases in column precipitable water occurs at higher irrigation concentrations (Fig. 8j). Enhanced low-level divergence from strong irrigation-induced cooling increases the subsidence of dry air aloft as evidenced by 850-hPa vertical velocity changes of $-0.14$ cm s$^{-1}$ over irrigated grid cells compared with $+0.007$ cm s$^{-1}$ over nonirrigated grid cells. Slight increases in precipitation occur with increasing irrigation fraction, but these increases are not statistically significant because of the small number of heavily irrigated grid cells (Fig. 8k).

### *c. Comparison of precipitation regimes*

Because drought years have the lowest antecedent soil moisture, the largest soil moisture, latent heating, and sensible heating changes occur during drought years over irrigated grid cells and overall (Table 3). Greater latent heating during drought years drives the greatest 2-m mixing ratio increase for irrigated grid cells (Table 3). Similarly, the strong decrease in sensible heating is coincident with the largest 2-m temperature decreases (Table 3). The fact that dewpoints increase the most during drought years means that CAPE increases are also the largest during drought years (Table 3). However, precipitable water increases are the lowest for drought years because of strong subsidence of dry air over irrigated areas, with an average 850-hPa vertical velocity of $-0.14$ cm s$^{-1}$ for irrigation simulations during drought years, compared with just $-0.04$ cm s$^{-1}$ for all years. Greater temperature decreases during drought years lead to the greatest increases in CIN (Table 3). Because of strong CIN increases and the small increase in precipitable water, the smallest increase in precipitation occurs over the region of study during drought years [2.85 mm (0.63%)] when considering all precipitation regimes. Meager precipitation increases during drought years are coincident with the greatest increase in ET (23.84 mm), meaning that irrigation results in the largest loss of water (20.99 mm) during drought years over the region of study. Similarly, large increases in CIN and relatively small increases in precipitable water over irrigated grid cells result in a precipitation decrease of 1.26 mm ($-0.31$%) over irrigated grid cells during drought years, in contrast with a large increase of 14.87 mm (3.01%) and 9.97 mm (1.77%) during normal and pluvial years, respectively. These precipitation decreases are coincident with the largest increase in ET (115.56 mm) over irrigated grid cells, meaning that irrigation results in the largest loss of water (116.82 mm) over irrigated grid cells during drought

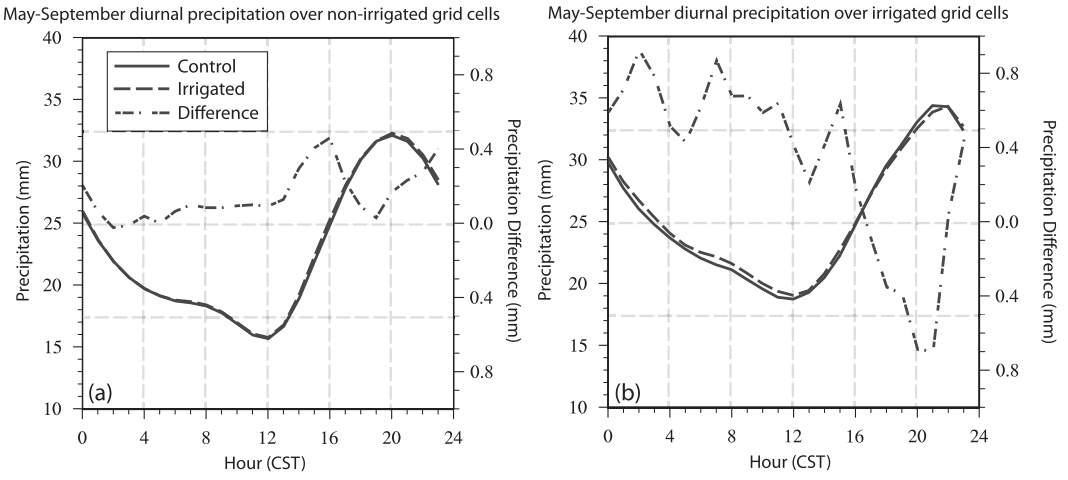


FIG. 7. Area-weighted average of May–September diurnal precipitation (mm; shown in central standard time) for all simulated years (control, irrigated, and difference) over (a) grid cells with less than 10% irrigation and over (b) grid cells with at least 10% irrigation over the region of study.

years. While a small precipitation decrease occurs over irrigated grid cells during drought years, a slight increase occurs over nonirrigated grid cells during drought years because of an increase in convergence and smaller increases in CIN compared with irrigated grid cells (Table 3).

The impacts of irrigation are also the most amplified with increasing irrigation fraction during drought years. The strongest increase in latent (Fig. 8b) and sensible heating (Fig. 8c) with increasing irrigation intensity occur during drought years, driving the greatest changes in 2-m temperature (Fig. 8d) and mixing ratio (Fig. 8e) with increasing irrigation fraction. Greater increases in mixing ratio for heavily irrigated grid cells during drought years result in greater CAPE increases with increasing irrigation fraction (Fig. 8f). However, strong temperature decreases over heavily irrigated grid cells lead to stronger CIN increases (Fig. 8g; not significant) with increasing irrigation fraction. Total column precipitable water increases also sharply decline with increasing irrigation fraction (Fig. 8j) because of increased subsidence of dry air over heavily irrigated grid cells (not shown). Amplified CIN increases and smaller increases in precipitable water over heavily irrigated grid cells result in a decrease in precipitation with increasing irrigation intensity during drought years (Fig. 8k), despite strong CAPE increases.

While the effects of irrigation are amplified during drought years, rather ambiguous effects occur during normal and pluvial years. The smallest changes in latent (Fig. 8b) and sensible heating (Fig. 8c) occur in heavily irrigated grid cells during normal years, which results in the smallest changes in 2-m temperature with increasing irrigation fraction (Fig. 8d). Weakened surface cooling over heavily irrigated grid cells limits the subsidence of dry air above irrigated areas (850-hPa vertical velocity of $-0.06$ cm s$^{-1}$ over irrigated grid cells during irrigation simulations of normal years compared with $-0.14$ cm s$^{-1}$ during drought years), allowing for greater increases in precipitable water over heavily irrigated grid cells (Fig. 8j). Despite the small CAPE increase (Fig. 8f) and the large CIN increase (Fig. 8g) with increasing irrigation fraction, precipitation increases with increasing irrigation intensity during normal years (Fig. 8k) because of precipitable water increases (Fig. 8j) and weak subsidence over heavily irrigated grid cells. Precipitation increases by 5.94 mm (1.06%) overall and by 14.87 mm (3.01%) for irrigated grid cells during normal years. Nonirrigated grid cells have smaller increases in precipitation during normal years [4.31 mm (0.76%)] despite strong increases in surface convergence and precipitable water because of relatively smaller increases in CAPE compared with other regimes (Table 3).

Pluvial years see the greatest precipitation increases when considering the entire region of study [6.14 mm (0.98%)] and nonirrigated grid cells [5.44 mm (0.85%)], with increases over irrigated grid cells [9.97 mm (1.77%)]. This is coincident with the smallest decrease in convergence overall and the smallest percentage decrease in convergence for irrigated grid cells (Table 3). CIN decreases during pluvial years on average over the entire region of study, while over irrigated grid cells the small increase in CIN is the smallest of the three precipitation regimes (Table 3).

### *d. Sensitivity simulations from time-decay irrigation technique*

Because the approach used to simulate intensive irrigation described in section 2b (ORIGINAL) used approximately twice as much water used as USDA

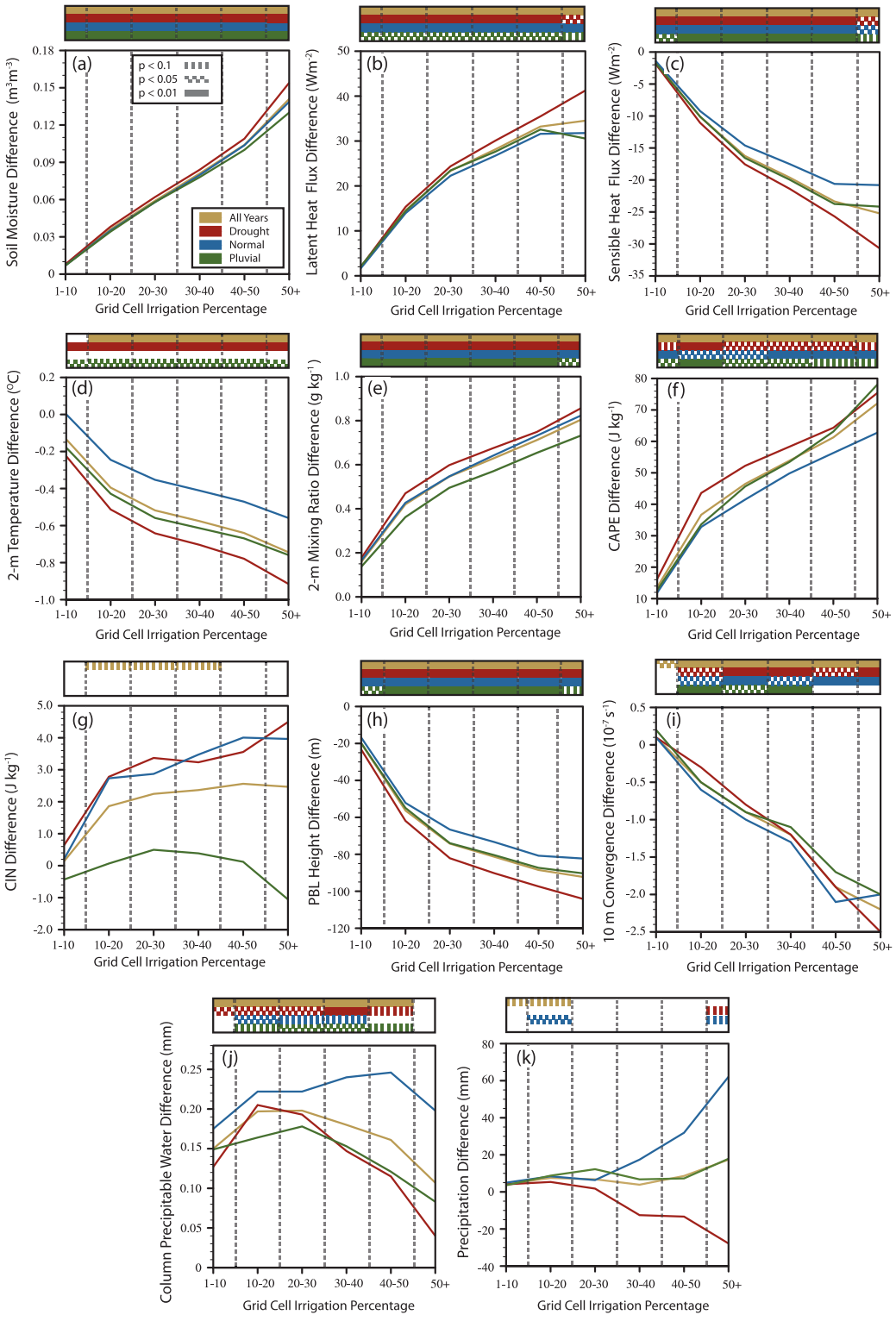


FIG. 8. Area-weighted average of IRRIG minus CTRL simulated (a) volumetric soil moisture content (kg kg$^{-1}$), (b) latent heat flux (W m$^{-2}$), (c) sensible heat flux (W m$^{-2}$), (d) 2-m temperature (°C), (e) 2-m mixing ratio (g kg$^{-1}$), (f) CAPE (J kg$^{-1}$), (g) CIN (J kg$^{-1}$), (h) PBL height (m), (i) 10-m convergence ($10^5$ s$^{-1}$), (j) column precipitable water (mm), and (k) precipitation (mm) as a function of gridcell irrigation fraction. Drought, normal, pluvial (flood), and all years are plotted as described in (a) along with levels of statistical significance. Only grid cells within the region of study were considered.

TABLE 3. May–September area-weighted averages of differences between control and irrigated simulations for all, drought, normal, and pluvial years. Area-weighted averages were calculated for the region of study, for grid cells with at least 10% irrigation within the region of study, and for grid cells with less than 10% irrigation within the region of study. Significance values for paired *t* tests are as follows: * ($p < 0.1$), ** ($p < 0.05$), and *** ($p < 0.01$).

| | Region of study | | | 10%+ irrigated grid cells in region of study | | | Grid cells with < 10% irrigation within RoS | | |
|---|---|---|---|---|---|---|---|---|---|
| | Drought | Normal | Pluvial | Drought | Normal | Pluvial | Drought | Normal | Pluvial |
| Irrigated area ($km^2$) | $6.39 \times 10^4$ | $6.39 \times 10^4$ | $6.39 \times 10^4$ | $5.0 \times 10^4$ | $5.0 \times 10^4$ | $5.0 \times 10^4$ | $1.83 \times 10^4$ | $1.83 \times 10^4$ | $1.83 \times 10^4$ |
| Soil moisture ($m^3\ m^{-3}$) | 0.0145 | 0.0138 | 0.0130 | 0.0623 | 0.0580 | 0.0560 | $5.80 \times 10^{-3}$ | $5.79 \times 10^{-3}$ | $5.24 \times 10^{-3}$ |
| | (6.40%)*** | (5.53%)*** | (5.19%)*** | (30.2%)*** | (26.1%)*** | (25.0%)*** | (2.52%)*** | (2.28%)*** | (2.04%)*** |
| Latent heat flux ($W\ m^{-2}$) | 4.508 | 3.940 | 4.431 | 22.291 | 19.695 | 20.250 | 1.278 | 1.079 | 1.559 |
| | (4.60%)*** | (3.84%)*** | (4.44%)** | (24.6%)*** | (20.9%)*** | (22.5%)** | (1.29%)** | (1.04%)*** | (1.53%)** |
| Sensible heat flux ($W\ m^{-2}$) | −3.587 | −2.842 | −3.276 | −16.115 | −12.948 | −14.562 | −1.312 | −1.007 | −1.227 |
| | (−7.68%)*** | (−7.00%)*** | (−8.59%)** | (−31.1%)*** | (−27.8%)*** | (−31.8%)*** | (−2.87%)*** | (−2.55%)*** | (−3.34%)* |
| Net radiation ($W\ m^{-2}$) | −0.081 | 0.181 | 0.223 | 1.171 | 2.452 | 1.118 | −0.308 | −0.231 | 0.060 |
| | (−0.04%) | (0.11%) | (0.13%) | (0.68%) | (1.45%)*** | (0.68%) | (−0.18%) | (−0.14%)* | (0.04%) |
| 2-m temperature (°C) | −0.247*** | −0.023 | −0.206** | −0.611*** | −0.326 | −0.519*** | −0.181*** | 0.032 | −0.150** |
| 2-m mixing ratio ($g\ kg^{-1}$) | 0.209 | 0.196 | 0.168 | 0.569 | 0.528 | 0.462 | 0.143 | 0.136 | 0.115 |
| | (1.95%)*** | (1.95%)*** | (1.51%)*** | (5.71%)*** | (5.62%) | (4.44%)*** | (1.32%)*** | (1.33%)*** | (1.02%)** |
| Precipitable water change (mm) | 0.115 | 0.159 | 0.136 | 0.177 | 0.224 | 0.156 | 0.104 | 0.148 | 0.133 |
| | (0.42%)** | (0.62%) | (0.46%) | (0.71%)*** | (0.94%)* | (0.59%)*** | (0.37%)** | (0.57%) | (0.45%) |
| CAPE ($J\ kg^{-1}$) | 18.963 | 13.949 | 15.470 | 50.971 | 40.456 | 43.870 | 13.150 | 9.135 | 10.312 |
| | (5.85%)** | (5.71%)*** | (3.90%)** | (19.4%)** | (18.8%)*** | (12.0%)** | (3.92%)* | (3.66%)* | (2.56%) |
| CIN ($J\ kg^{-1}$) | 0.743 | 0.394 | −0.495 | 3.147 | 3.024 | 0.104 | 0.306 | −0.084 | −0.604 |
| | (2.14%) | (1.32%) | (−1.22%) | (9.12%) | (9.44%) | (0.24%) | (0.88%) | (−0.28%) | (−1.50%) |
| PBL height (m) | −26.579 | −20.333 | −23.687 | −75.017 | −61.835 | −66.711 | −17.78 | −12.796 | −15.874 |
| | (−3.15%)*** | (−2.61%)*** | (−2.85%)** | (−8.37%)*** | (−7.44%)*** | (−7.55%)** | (−2.13%)*** | (−1.66%)*** | (1.93%)** |
| LFC (m) | −201.73 | −130.15 | −132.77 | −446.03 | −279.00 | −275.43 | −157.367 | −103.110 | −106.862 |
| | (−2.91%)** | (−1.66%)* | (−2.17%)** | (−5.94%)** | (−3.53%)** | (−4.38%)*** | (−2.31%)** | (−1.32%)* | (−1.75%)** |
| Convergence ($10^{-9}\ s\text{-}^1$) | $-4.08 \times 10^{-9}$ | $-3.46 \times 10^{-9}$ | $-2.29 \times 10^{-9}$ | $-8.16 \times 10^{-8}$ | $-9.63 \times 10^{-8}$ | $-8.81 \times 10^{-8}$ | $1.00 \times 10^{-8}$ | $1.34 \times 10^{-8}$ | $1.33\ 10^{-8}$ |
| | (−5.68%) | (−17.5%) | (−1.99%) | (−114%)*** | (−188%)*** | (−45.5%)** | (13.9%) | (95.3%) | (13.2%) |
| Precipitation change (mm) | 2.850 | 5.935 | 6.136 | −1.258 | 14.866 | 9.973 | 3.596 | 4.313 | 5.439 |
| | (0.63%) | (1.06%) | (0.98%)* | (−0.31%) | (3.01%)** | (1.77%) | (0.78%) | (0.76%) | (0.85%)*** |

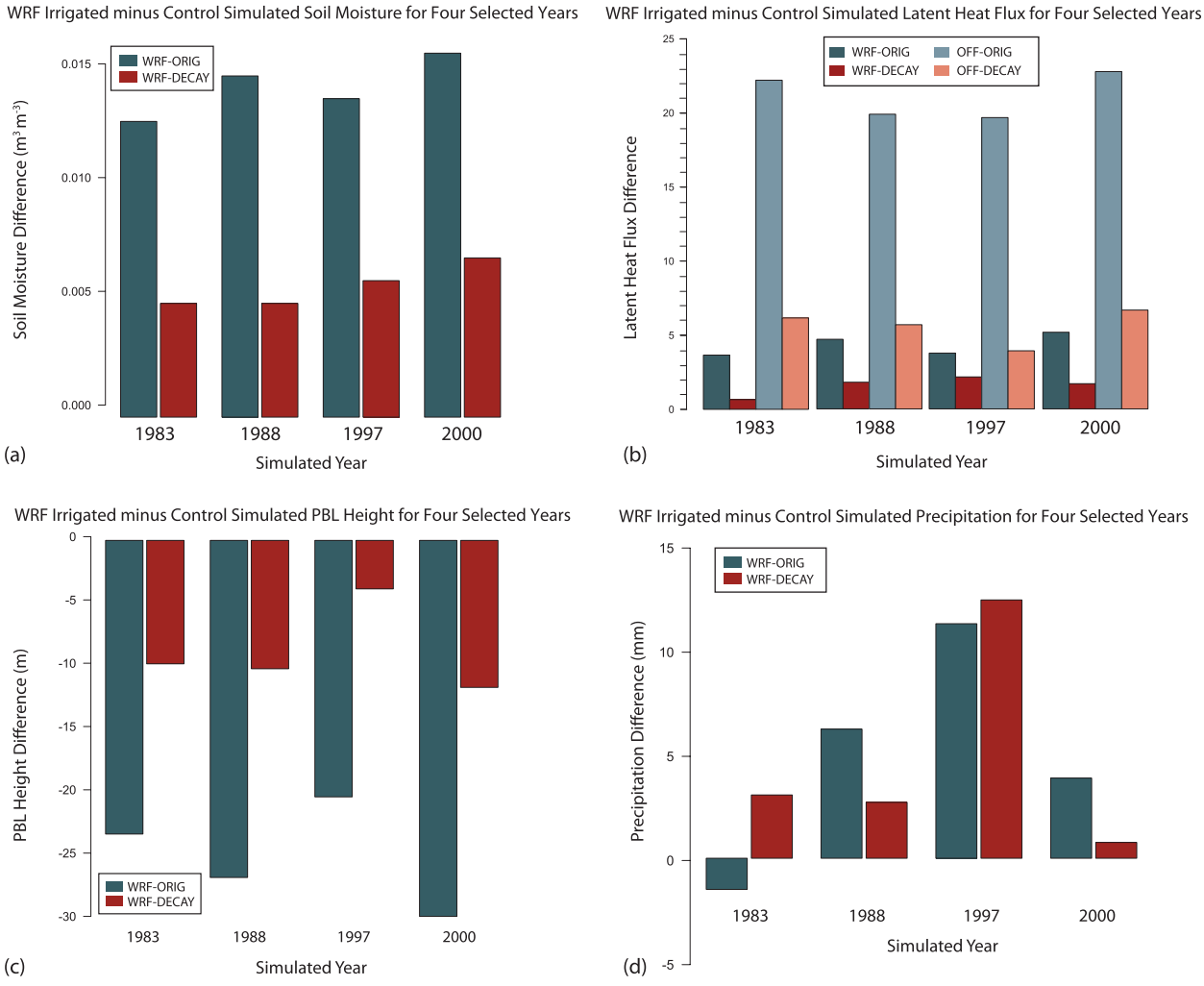


FIG. 9. Area-weighted average of IRRIG minus CTRL simulated (a) volumetric soil moisture (kg kg$^{-1}$) within the region of study for simulations of original irrigation method (ORIGINAL) and time-decay irrigation method (DECAY). (b) As in (a), but for latent heat flux (W m$^{-2}$) with the inclusion of offline (OFF) simulations as described in section 4b. (c) As in (a), but for PBL height (m). (d) As in (a), but for precipitation (mm).

estimates, sensitivity simulations with a time-decay irrigation (DECAY) scheme were conducted to determine whether the overuse of water in this study exaggerates the atmospheric response. WRF simulations using the ORIGINAL approach are referred to as WRF-ORIG in this section and section 4b, while WRF simulations using the DECAY scheme are referred to as WRF-DECAY. In WRF-DECAY simulations, the soil moisture in the irrigated portion of grid cells was set at saturation whenever it dropped below 50% of saturation. Results from WRF-DECAY simulations of 4 years (2 drought, 1 normal, and 1 pluvial) are compared with the same 4 years simulated in WRF-ORIG simulations and described below.

Similar May–September precipitation differences occur between irrigated and control simulations (4.71 mm for WRF-DECAY compared to 4.95 mm for WRF-ORIG) despite the fact that soil moisture changes in WRF-DECAY simulations are only 41% as large as WRF-ORIG simulations (Fig. 9a). Overall changes in latent heating are only 36% as large as WRF-ORIG simulations (Fig. 9b), which contributes to dewpoint temperature changes that are 39% as large. Although CAPE increases are only 35% as large, WRF-DECAY simulations result in slightly smaller increases in precipitation (Fig. 9d) compared to WRF-ORIG simulations (1.02% compared with 1.07%). Changes in latent heating and temperature from WRF-ORIG simulations are similar to results from previous observational and modeling studies as discussed in section 4a, while changes in temperature and latent heating from WRF-DECAY simulations are significantly smaller. Simulated changes in latent heat flux and 2-m

temperature in WRF-ORIG compare reasonably well with Ameriflux observations in Nebraska (section 3a). Based on these findings, the ORIGINAL approach is determined to be an accurate representation of the atmospheric effect on irrigation in WRF despite overusing water and being conceptually unrealistic. Because such an extreme irrigation approach was required to achieve accurate changes in surface fluxes, further work examining the atmospheric response to managed ecosystems and irrigation in WRF will likely need a more realistic and robust representation of agriculture and irrigation.

## 4. Discussion

### *a. Comparison to previous studies*

Overall, simulated latent heating changes from irrigation compare reasonably well with previous studies despite the overuse of water. June–August average simulated latent heating increases of 21 W $m^{-2}$ over irrigated grid cells are similar to simulated increases of 20–30 W $m^{-2}$ over the Great Plains from Sacks et al. (2009). Simulated latent heating increases averaged over Nebraska are only 6.53 W $m^{-2}$ (5.9%) for the period of 7–15 July 1997 (not shown) compared with 27 W $m^{-2}$ (35%) over the same period as Adegoke et al. (2003). August latent heating increases of up to ~35 W $m^{-2}$ occur over heavily irrigated grid cells in Nebraska (not shown), compared with up to 100 W $m^{-2}$ in offline simulations from Ozdogan et al. (2010).

Temperature changes over heavily irrigated grid cells are generally the same as previous studies, while dewpoint changes are somewhat smaller. Mahmood et al. (2006) observed a 4°–5°C growing-season dewpoint temperature difference between irrigated and nonirrigated sites in Nebraska—well above the 1.5°C differences over similar heavily irrigated grid cells found in this study. Adegoke et al. (2003) simulated a 2.6°C dewpoint temperature increase over Nebraska, compared with a 0.53°C increase for the same period in this study. Simulated May–September 2-m temperature decreases of up to 0.9°C occur for all simulated years over the most heavily irrigated areas in the model domain, compared with observed growing-season temperature decreases of ~1°C for heavily irrigated sites in Nebraska during the second half of the twentieth century (Mahmood et al. 2006). June–August simulated temperature decreases of up to 0.9°C over the most heavily irrigated grid cells in Nebraska are smaller than the 2°C temperature decrease reported by Sacks et al. (2009).

Small but statistically significant precipitation increases of 1.29% occur from June to August, compared with a 1.24% June–August precipitation increase globally over land reported by Sacks et al. (2009). DeAngelis et al. (2010) observed a larger precipitation increase of approximately 1.7% over the Great Plains and Midwest (regions 1–3 in DeAngelis et al. 2010) for May–September due to irrigation, while Segal et al. (1998) simulated a smaller 0.68% continentally averaged increase over the United States using a low-resolution mesoscale model. In general, precipitation changes in this study are similar to previous studies despite the fact that temperature and dewpoint temperature changes are generally smaller. Although this approach overused water, the surface and atmospheric responses are of a similar magnitude to previous studies.

### *b. Comparison with offline simulations*

Because of the large difference in latent heating changes in this study with those from Ozdogan et al. (2010), offline simulations of the Noah LSM were conducted to assess the validity of using offline simulations to simulate the impacts of irrigation on the energy and water budgets. Offline simulations were conducted using the High-Resolution Land Data Assimilation System (HRLDAS) for all identified years (Chen et al. 2004). Separate offline irrigation simulations were run using the irrigation technique described in section 2b (ORIGINAL) and the time-decay irrigation technique described in section 3d (DECAY).

Offline simulations of the Noah LSM using the ORIGINAL technique (hereafter referred to as OFF-ORIG) show a greater overestimation of latent heating from irrigation compared with Ozdogan et al. (2010). Over the region of study, average May–September latent heating changes from OFF-ORIG simulations of four individual years (the same years simulated in WRF-DECAY simulations) are 388% larger than WRF-ORIG simulations (Fig. 9b). OFF-ORIG simulations result in May–September latent heat flux changes of up to 280 W $m^{-2}$ for heavily irrigated grid cells averaged over all simulated years (Fig. 10b), compared with up to 47 W $m^{-2}$ from WRF-ORIG simulations (Fig. 4a). Latent heating increases by up to 95 W $m^{-2}$ in OFF-DECAY simulations (Fig. 10a), which is significantly smaller than OFF-ORIG simulations (Fig. 10b). However, average latent heating changes from the OFF-DECAY simulations are still 29.7% larger than values from WRF-ORIG simulations (Fig. 9b). These results show that overestimation of the latent heating change in offline simulations occurs because the atmosphere cannot respond to a greater flux of moisture from the surface with irrigation. This results in an unrealistically large water vapor gradient that drives exaggerated latent heat flux values over irrigated fields.

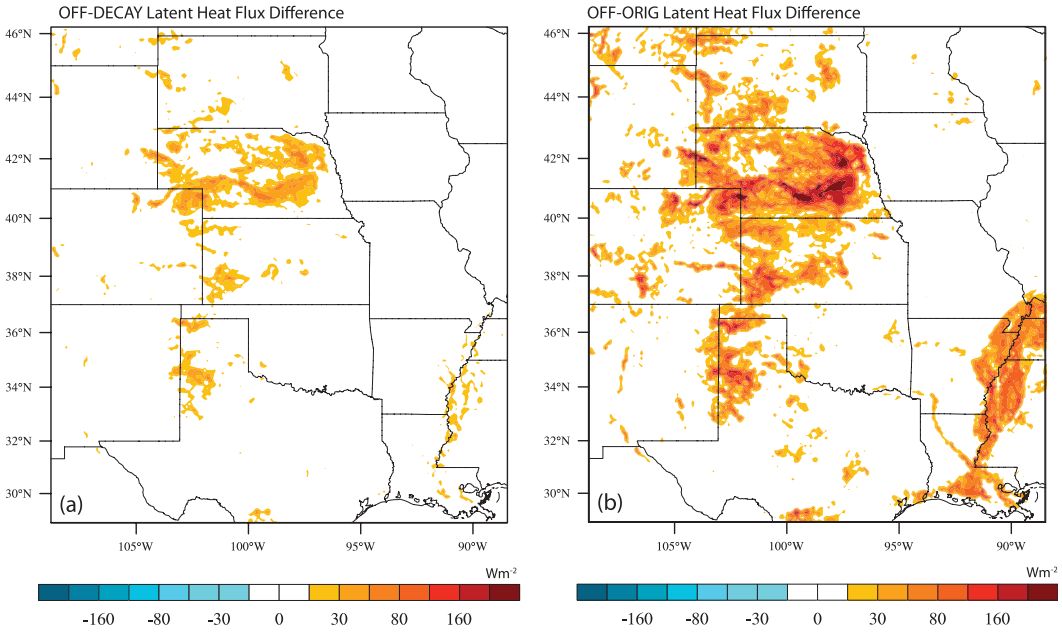


FIG. 10. Average May–September IRRIG minus CTRL simulated latent heat flux (W $m^{-2}$) for all simulated years using offline (OFF) simulations that employed (a) the DECAY irrigation technique from section 3d (OFF-DECAY) and (b) the ORIGINAL irrigation technique from section 2b (OFF-ORIG).

### c. *Overall impact of irrigation on Great Plains precipitation*

Simulation of irrigation alters the energy budget and surface temperature and moisture over the Great Plains by partitioning net radiation into additional latent heating at the expense of sensible heating. These changes have opposing effects on the development of precipitation and the forcing of convection. When considering how irrigation affects the development of convection, changes in CAPE, CIN, and precipitable water play a leading role. CAPE and precipitable water increases lead to more precipitation over the study area and over irrigated grid cells for the average of all simulated years despite increases in CIN. Because precipitation increases occur for both irrigated and nonirrigated grid cells, the enhancement of convection from increased low-level moisture with irrigation overwhelms the suppression of convection from irrigation-induced cooling over the Great Plains. While irrigation results in precipitation increases, ET increases are much larger, resulting in a net loss of water over the Great Plains. Despite larger increases in CIN over irrigated grid cells, precipitation increases are greater over irrigated areas compared with the region of study and nonirrigated grid cells because of stronger CAPE and precipitable water increases, which is similar to results as reported by Sacks et al. (2009). Increases in surface divergence over irrigated areas suppress convection in the late afternoon and early evening (Fig. 7b) when convection is more surface based. Conversely, large nocturnal precipitation increases occur when convection is elevated above the nocturnal boundary layer (Wilson and Roberts 2006). During these times, the elevated convection, which is decoupled from the surface, is not influenced by surface cooling and divergence. Therefore, nocturnal convective precipitation increases only as a result of additional precipitable water and low-level moisture. In contrast, nonirrigated grid cells see increases in precipitation because of large increases in surface convergence during the late afternoon hours when convection is frequently surface based (Wilson and Roberts 2006). However, overall increases in convective precipitation are not as large over nonirrigated grid cells because of less CAPE and precipitable water. The fact that greater increases in precipitation occur over irrigated grid cells during periods when convection is elevated suggests that irrigation has a greater impact on elevated convection that forms above the nocturnal boundary layer.

Irrigation becomes more influential with increasing irrigation fraction. As the gridcell irrigation fraction increases, greater changes to latent and sensible heating result in stronger temperature and mixing ratio changes. Despite the 2-m mixing ratio increase with increasing irrigation intensity, total column precipitable water decreases with increasing irrigation fraction for heavily irrigated grid cells. This occurs because increased subsidence above irrigated areas results in drier air aloft,

reducing the column-integrated precipitable water. Regardless, large 2-m mixing ratio increases over heavily irrigated grid cells drive large increases in CAPE with increasing irrigation intensity. Similarly, stronger irrigation-induced cooling with increasing irrigation fraction results in greater CIN increases over heavily irrigated grid cells. The enhanced CIN increases with increasing irrigation fraction are more than offset by strong CAPE increases. As a result, a slight precipitation increase (not significant) occurs on average for all simulated years as irrigation intensity increases.

Factors that affect the suppression and enhancement of convection from irrigation are not constant when considering variations in antecedent soil moisture. Irrigation has a stronger impact on the surface energy and moisture budgets during periods with low antecedent soil moisture. Greater water vapor deficits over irrigated fields during drought years result in larger latent heating increases over irrigated areas. As a result, greater irrigation-induced cooling and enhancement of surface moisture occurs during drought years. While CAPE increases are the largest during drought years, precipitation decreases over irrigated grid cells because of large CIN increases and strong subsidence. Similarly, precipitation decreases with increasing irrigation intensity during drought years because of strong CIN increases, precipitable water declines, and large increases in subsidence with increasing irrigation fraction.

The fact that precipitation decreases over irrigated grid cells during drought years suggests that the level of antecedent soil moisture is a control for whether irrigation results in suppression or enhancement of convection. For periods when the antecedent soil moisture is extremely low, irrigation suppresses convection over irrigated areas. During these times, CIN increases and subsidence from irrigation-induced cooling overwhelm the enhancement of CAPE and precipitable water from increases in surface moisture. By contrast, irrigation contributes to stronger convection over irrigated areas when antecedent soil moisture is reasonably high because the enhancement in CAPE overwhelms the weaker CIN increases. This is supported by the fact that precipitation increases occur over irrigated grid cells in the region of study for normal and pluvial years, but not for drought years. Because irrigation has opposing effects on precipitation over irrigated areas at low and high antecedent soil moisture levels, an antecedent soil moisture threshold likely exists where the opposing effects of irrigation cancel one another. During periods when the antecedent soil moisture is below the threshold, irrigation suppresses the development of convective precipitation over irrigated areas. For years when antecedent soil moisture is above the threshold, irrigation enhances convective precipitation over irrigated areas.

## 5. Conclusions

Irrigation has expanded over the Great Plains since World War II, threatening the sustainability of regional groundwater supplies. Because of large groundwater withdrawals from irrigation, declines in the water table have increased costs for agricultural and municipal water use (McGuire et al. 2003). In this paper, irrigation has been shown to impact the water cycle over the Great Plains by enhancing evapotranspiration and precipitation. Increases in evapotranspiration were found to be much larger than increases in precipitation, confirming that irrigation enhances the net loss of water over the Great Plains. Irrigation was shown to have the greatest impact on convection elevated above the nocturnal boundary layer, resulting in greater increases in precipitation over irrigated grid cells.

The effects of irrigation have also been shown to depend on the level of antecedent soil moisture. During periods with high antecedent soil moisture, irrigation enhanced precipitation (especially over irrigated cells), whereas when antecedent soil moisture was low, precipitation over irrigated cells was suppressed. Therefore, an antecedent soil moisture threshold likely separates conditions where irrigation results in either the enhancement or the suppression of convective precipitation. Knowledge of possible conditions when irrigation suppresses precipitation could be critical for effectively managing regional groundwater supplies. Years with low antecedent soil moisture require the largest volume of water for irrigation while at the same time experiencing decreases in precipitation over irrigated areas. For these reasons, irrigation potentially has the most negative impact on groundwater supplies during drought years. The combination of high drought sensitivity and future projections of increased drought likelihood with climate change over the Great Plains (Gregory et al. 1997; Solomon et al. 2007; Kumar 2007; Manabe et al. 2004; Rind et al. 1990; Wang 2005; Wetherald and Manabe 1995, 1999) suggest that irrigation might further stress groundwater supplies in the region.

In a region where drought severity, frequency, and persistence are expected to increase with climate change, it is important that we understand the impact that irrigation has on the water cycle so that we can effectively manage water resources. Part II of this paper (Harding and Snyder 2012) examines where water that is added to irrigated fields eventually falls as precipitation, allowing for additional understanding of the impact that irrigation has on the water budget. Improved

understanding will be useful for assisting those who will be tasked with developing water management and conservation plans for the Great Plains, helping to reverse recent depletion of groundwater supplies, and ensuring a more economically viable supply of groundwater in one of the world's most important agricultural regions.

*Acknowledgments.* Support for this project was provided by the University of Minnesota Grant-in-Aid Program (Grant 21601). This work was carried out in part using computing resources at the University of Minnesota Supercomputing Institute. We thank Dr. Mutlu Ozdogan for providing the fractional irrigation dataset, Dr. Shashi Verma for use of the Ameriflux data at his Mead, Nebraska, sites, and Dr. Stefan Liess for help with the coupled model enhancements. The authors are indebted to two anonymous reviewers for their comprehensive and constructive comments on this manuscript.

## REFERENCES

Adegoke, J. O., R. A. Pielke, J. Eastman, R. Mahmood, and K. G. Hubbard, 2003: Impact of irrigation on midsummer surface fluxes and temperature under dry synoptic conditions: A regional atmospheric model study of the U.S. High Plains. *Mon. Wea. Rev.,* **131,** 556–564.

Baidya Roy, S., G. C. Hurtt, C. P. Weaver, and S. W. Pacala, 2003: Impact of historical land cover change on the July climate of the United States. *J. Geophys. Res.,* **108,** 4793, doi:10.1029/2003JD003565.

Banacos, P. C., and D. M. Schultz, 2005: The use of moisture flux convergence in forecasting convective initiation: Historical and operational perspectives. *Wea. Forecasting,* **20,** 351–366.

Barnston, A. G., and P. T. Schickedanz, 1984: The effect of irrigation on warm season precipitation in the southern Great Plains. *J. Climate Appl. Meteor.,* **23,** 865–888.

Betts, R. A., P. M. Cox, S. E. Lee, and F. I. Woodward, 1997: Contrasting physiological and structural vegetation feedbacks in climate change simulations. *Nature,* **387,** 796–799.

Bluestein, H. B., 1993: *Observations and Theory of Weather Systems.* Vol. 2, *Synoptic-Dynamic Meteorology in Midlatitudes,* Oxford University Press, 594 pp.

Boucher, O., G. Myhre, and A. Myhre, 2004: Direct human influence of irrigation on atmospheric water vapour and climate. *Climate Dyn.,* **22,** 597–603.

Changnon, S. A., 2001: Thunderstorm rainfall in the conterminous United States. *Bull. Amer. Meteor. Soc.,* **82,** 1925–1940.

Chen, F., and J. Dudhia, 2001: Coupling an advanced land surface–hydrology model with the Penn State–NCAR MM5 modeling system. Part I: Model implementation and sensitivity. *Mon. Wea. Rev.,* **129,** 569–585.

——, K. W. Manning, D. N. Yates, M. A. LeMone, S. B. Trier, R. Cuenca, and D. Niyogi, 2004: Development of high resolution land data assimilation system and its application to WRF. Preprints, *16th Conf. on Numerical Weather Prediction,* Seattle, WA, Amer. Meteor. Soc., 22.3. [Available online at https://ams.confex.com/ams/84Annual/techprogram/paper_67333.htm.]

Crook, N. A., 1996: Sensitivity of moist convection forced by boundary layer processes to low-level thermodynamic fields. *Mon. Wea. Rev.,* **124,** 1767–1785.

DeAngelis, A., F. Dominguez, Y. Fan, A. Robock, M. D. Kustu, and D. Robinson, 2010: Evidence of enhanced precipitation due to irrigation over the Great Plains of the United States. *J. Geophys. Res.,* **115,** D15115, doi:10.1029/2010JD013892.

De Ridder, K., and H. Gallée, 1998: Land surface–induced regional climate change in southern Israel. *J. Appl. Meteor.,* **37,** 1470–1485.

Dudhia, J., 1989: Numerical study of convection observed during the Winter Monsoon Experiment using a mesoscale two-dimensional model. *J. Atmos. Sci.,* **46,** 3077–3107.

Findell, K. L., and E. A. B. Eltahir, 2003a: Atmospheric controls on soil moisture–boundary layer interactions. Part I: Framework development. *J. Hydrometeor.,* **4,** 552–569.

——, and ——, 2003b: Atmospheric controls on soil moisture–boundary layer interactions. Part II: Feedbacks within the continental United States. *J. Hydrometeor.,* **4,** 570–583.

Friedl, M., and Coauthors, 2002: Global land cover mapping from MODIS: Algorithms and early results. *Remote Sens. Environ.,* **83,** 287–302.

Gregory, J. M., J. F. B. Mitchell, and A. J. Brady, 1997: Summer drought in northern midlatitudes in a time-dependent $CO_2$ climate experiment. *J. Climate,* **10,** 662–686.

Harding, K. J., and P. K. Snyder, 2012: Modeling the atmospheric response to irrigation in the Great Plains. Part II: The precipitation of irrigated water and changes in precipitation recycling. *J. Hydrometeor.,* **13,** 1686–1702.

Higgins, R. W., W. Shi, E. Yarosh, and R. Joyce, 2000: Improved United States precipitation quality control system and analysis. NCEP/Climate Prediction Center ATLAS 7, 40 pp.

Hong, S. B., V. Lakshmi, E. E. Small, F. Chen, M. Tewari, and K. W. Manning, 2009: Effects of vegetation and soil moisture on the simulated land surface processes from the coupled WRF/Noah model. *J. Geophys. Res.,* **114,** D18118, doi:10.1029/2008JD011249.

Hong, S. Y., Y. Noh, and J. Dudhia, 2006: A new vertical diffusion package with an explicit treatment of entrainment processes. *Mon. Wea. Rev.,* **134,** 2318–2341.

Hutson, S. S., N. L. Barber, J. F. Kenny, K. S. Linsey, D. S. Lumia, and M. A. Maupin, 2004: Estimated use of water in the United States in 2000. U.S. Geological Survey Circular 1268, 46 pp.

Jacquemin, B., and J. Noilhan, 1990: Sensitivity study and validation of a land surface parameterization using the HAPEX-MOBILHY data set. *Bound.-Layer Meteor.,* **52,** 93–134.

Jódar, J., J. Carrera, and A. Cruz, 2010: Irrigation enhances precipitation at the mountains downwind. *Hydrol. Earth Syst. Sci.,* **14,** 2003–2010.

Kain, J. S., and Coauthors, 2008: Some practical considerations regarding horizontal resolution in the first generation of operational convection-allowing NWP. *Wea. Forecasting,* **23,** 931–952.

Kanamitsu, M., W. Ebisuzaki, J. Woollen, S. K. Yang, J. J. Hnilo, M. Fiorino, and G. L. Potter, 2002: NCEP–DOE AMIP-II Reanalysis (R-2). *Bull. Amer. Meteor. Soc.,* **83,** 1631–1643.

Koster, R. D., and Coauthors, 2004: Regions of strong coupling between soil moisture and precipitation. *Science,* **305,** 1138–1140.

Kueppers, L. M., M. A. Snyder, and L. C. Sloan, 2007: Irrigation cooling effect: Regional climate forcing by land-use change. *Geophys. Res. Lett.,* **34,** L03703, doi:10.1029/2006GL028679.

Kumar, S., 2007: Fourth assessment report of the Intergovernmental Panel on Climate Change: Important observations and conclusions. *Curr. Sci.,* **92,** 1034.

Lee, E., W. Sacks, T. Chase, and J. Foley, 2011: Simulated impacts of irrigation on the atmospheric circulation over Asia. *J. Geophys. Res.,* **116,** D08114, doi:10.1029/2010JD014740.

Lin, Y., and K. Mitchell, 2005: The NCEP stage II/IV hourly precipitation analyses: Development and applications. Preprints, *19th Conf. on Hydrology,* San Diego, CA, Amer. Meteor. Soc., 1.2. [Available online at https://ams.confex.com/ams/Annual2005/techprogram/paper_83847.htm.]

Lobell, D. B., G. Bala, and P. B. Duffy, 2006: Biogeophysical impacts of cropland management changes on climate. *Geophys. Res. Lett.,* **33,** L06708, doi:10.1029/2005GL025492.

Mahmood, R., K. G. Hubbard, and C. Carlson, 2004: Modification of growing-season surface temperature records in the northern Great Plains due to land-use transformation: Verification of modelling results and implication for global climate change. *Int. J. Climatol.,* **24,** 311–327.

——, S. A. Foster, T. Keeling, K. G. Hubbard, C. Carlson, and R. Leeper, 2006: Impacts of irrigation on 20th century temperature in the northern Great Plains. *Global Planet. Change,* **54,** 1–18.

Manabe, S., R. Wetherald, P. Milly, T. Delworth, and R. Stouffer, 2004: Century-scale change in water availability: $CO_2$-quadrupling experiment. *Climatic Change,* **64,** 59–76.

McGuire, V. L., 2007: Water-level changes in the High Plains aquifer, predevelopment to 2005 and 2003 to 2005. U.S. Geological Survey Scientific Investigations Rep. 2006-5324, 7 pp.

——, M. R. Johnson, R. L. Schieffer, J. S. Stanton, S. K. Sebree, and I. M. Verstraeten, 2003: Water in storage and approaches to ground-water management, High Plains aquifer, 2000. U.S. Geological Survey Circular 1243, 51 pp.

Mesinger, F., and Coauthors, 2006: North American Regional Reanalysis. *Bull. Amer. Meteor. Soc.,* **87,** 343–360.

Mlawer, E. J., S. J. Taubman, P. D. Brown, M. J. Iacono, and S. A. Clough, 1997: Radiative transfer for inhomogeneous atmospheres: RRTM, a validated correlated-*k* model for the longwave. *J. Geophys. Res.,* **102** (D14), 16 663–16 682.

Moore, N., and S. Rojstaczer, 2001: Irrigation-induced rainfall and the great plains. *J. Appl. Meteor.,* **40,** 1297–1309.

Morrison, H., G. Thompson, and V. Tatarskii, 2009: Impact of cloud microphysics on the development of trailing stratiform precipitation in a simulated squall line: Comparison of one- and two-moment schemes. *Mon. Wea. Rev.,* **137,** 991–1007.

NASS, 2002: Farm and ranch irrigation survey. *Geographic Area Series,* Vol. I, *2002 Census of Agriculture,* United States Department of Agriculture [Available online at http://www.nass.usda.gov/Census/Create_Census_FRIS.jsp.]

Noilhan, J., and S. Planton, 1989: A simple parameterization of land surface processes for meteorological models. *Mon. Wea. Rev.,* **117,** 536–549.

Ozdogan, M., and G. Gutman, 2008: A new methodology to map irrigated areas using multi-temporal MODIS and ancillary data: An application example in the continental US. *Remote Sens. Environ.,* **112,** 3520–3537.

——, M. Rodell, H. K. Beaudoing, and D. L. Toll, 2010: Simulating the effects of irrigation over the United States in a land surface model based on satellite-derived agricultural data. *J. Hydrometeor.,* **11,** 171–184.

Pielke, R. A., 2001: Influence of the spatial distribution of vegetation and soils on the prediction of cumulus convective rainfall. *Rev. Geophys.,* **39,** 151–177.

——, T. J. Lee, J. H. Copeland, J. L. Eastman, C. L. Ziegler, and C. A. Finley, 1997: Use of USGS-provided data to improve weather and climate simulations. *Ecol. Appl.,* **7,** 3–21.

Puma, M. J., and B. I. Cook, 2010: Effects of irrigation on global climate during the 20th century. *J. Geophys. Res.,* **115,** D16120, doi:10.1029/2010JD014122.

Rind, D., R. Goldberg, J. Hansen, C. Rosenzweig, and R. Ruedy, 1990: Potential evapotranspiration and the likelihood of future drought. *J. Geophys. Res.,* **95** (D7), 9983–10 004.

Sacks, W. J., B. I. Cook, N. Buenning, S. Levis, and J. H. Helkowski, 2009: Effects of global irrigation on the near-surface climate. *Climate Dyn.,* **33,** 159–175.

Segal, M., Z. Pan, R. W. Turner, and E. S. Takle, 1998: On the potential impact of irrigated areas in North America on summer rainfall caused by large-scale systems. *J. Appl. Meteor.,* **37,** 325–331.

Skamarock, W. C., and Coauthors, 2008: A description of the Advanced Research WRF version 3. NCAR Tech. Note NCAR/TN-475+STR, 113 pp.

Solomon, S., D. Qin, M. Manning, M. Marquis, K. Averyt, M. M. B. Tignor, H. L. Miller Jr., and Z. Chen, Eds., 2007: *Climate Change 2007: The Physical Science Basis.* Cambridge University Press, 996 pp.

Trenberth, K. E., A. Dai, R. M. Rasmussen, and D. B. Parsons, 2003: The changing character of precipitation. *Bull. Amer. Meteor. Soc.,* **84,** 1205–1217.

Twine, T. E., and Coauthors, 2000: Correcting eddy-covariance flux underestimates over a grassland. *Agric. For. Meteor.,* **103,** 279–300.

——, C. J. Kucharik, and J. A. Foley, 2005: Effects of El Niño–Southern Oscillation on the climate, water balance, and streamflow of the Mississippi River basin. *J. Climate,* **18,** 4840–4861.

Verma, S., and Coauthors, 2005: Annual carbon dioxide exchange in irrigated and rainfed maize-based agroecosystems. *Agric. For. Meteor.,* **131,** 77–96.

Wang, G., 2005: Agricultural drought in a future climate: Results from 15 global climate models participating in the IPCC 4th assessment. *Climate Dyn.,* **25,** 739–753.

Wetherald, R. T., and S. Manabe, 1995: The mechanisms of summer dryness induced by greenhouse warming. *J. Climate,* **8,** 3096–3108.

——, and ——, 1999: Detectability of summer dryness caused by greenhouse warming. *Climatic Change,* **43,** 495–511.

Wilson, J. W., and R. D. Roberts, 2006: Summary of convective storm initiation and evolution during IHOP: Observational and modeling perspective. *Mon. Wea. Rev.,* **134,** 23–47.

Wilson, K., and Coauthors, 2002: Energy balance closure at FLUXNET sites. *Agric. For. Meteor.,* **113,** 223–243.